



Effect of thermophoresis and its mathematical models on the transport and deposition of aerosol particles in natural convective flow on vertical and horizontal plates



Abhijit Guha*, Subho Samanta

Mechanical Engineering Department, Indian Institute of Technology Kharagpur, Kharagpur 721302, India

ARTICLE INFO

Article history:

Received 14 February 2014

Received in revised form

4 June 2014

Accepted 5 June 2014

Available online 20 June 2014

Keywords:

Deposition

Natural convection

Thermophoresis

Aerosol particles

ABSTRACT

An analysis is performed to study aerosol particle transport and deposition onto an isothermal horizontal or vertical plate due to the combined effects of laminar natural convection, Brownian diffusion and thermophoresis. Four configurations are considered: flow above a heated horizontal plate, flow beneath a cold horizontal plate, flow due to a heated vertical plate and that due to a cold vertical plate. Nano- to micro-sized particles (particle diameter in the range 1 nm to 5 μm) in air are considered. It is found that the deposition velocity decreases with an increase in particle diameter d_p (i.e. an increase in particle Schmidt number Sc), and increases with a decrease in the value of non-dimensional temperature difference $\Delta\hat{T}$ (from positive to negative values). For a downward-facing cold horizontal plate or cooled vertical plate, the thermal drift of particles assists Brownian diffusion which enhances deposition velocity. For an upward facing heated horizontal plate or heated vertical plate, the thermal drift away from the surface decreases the overall deposition velocity which decreases drastically above a certain particle size. It is shown that the thermal drift may enhance the deposition rate by several orders of magnitude under certain circumstances. The profound role of using different expressions for the thermophoretic force coefficient (κ) is assessed. It is found that the deposition velocity calculated using the expression for κ suggested by Talbot et al. (1980) is always higher than the values predicted by employing the expression proposed by Beresnev and Chernyak (1995). The difference in the calculated deposition velocity for the two thermophoretic models is significant when the particle diameter d_p is large and the fluid to particle thermal conductivity ratio λ_r is small. For example, at $d_p \sim 1 \mu\text{m}$, the Talbot et al. model may overpredict the deposition velocity by a factor 3, and at $d_p \sim 5 \mu\text{m}$, the Talbot et al. model may overpredict the deposition velocity by a factor 10. There is negligible difference between the two models when $d_p < 100 \text{ nm}$.

© 2014 Elsevier Ltd. All rights reserved.

1. Introduction

Particles suspended in a fluid stream may move for various reasons. The motion may be due to viscous drag, Brownian diffusion, gravitational settling, inertia, and electrical or other body forces. A diffusive mass flux may also arise due to a gradient in fluid temperature: suspended particles usually tend to move from regions of high temperature to low temperature. The force which

* Corresponding author. Tel.: +91 3222 281768; fax: +91 3222 282278.

E-mail address: a.guha@mech.iitkgp.ernet.in (A. Guha).

Nomenclature		Greek	
C_c	Cunningham correction	α	thermal diffusivity
d_p	diameter of particles	β	coefficient of thermal expansion at the reference temperature
D_B	Brownian diffusivity	η	similarity variable
D_T	coefficient of temperature-gradient driven diffusion	κ	thermophoretic force coefficient
f	reduced stream function	λ	thermal conductivity
g	gravitational acceleration	λ_r	thermal conductivity ratio ($\lambda_r \equiv \lambda_f/\lambda_p$)
Gr_x	Grashof number defined as $Gr_x = (g\beta T_w - T_\infty x^3)/\nu^2$	μ	dynamic viscosity of fluid
h	reduced pressure difference	ν	kinematic viscosity of fluid
J	flux of particles	ϕ	non-dimensional concentration ($\phi = N/N_\infty$)
k	Boltzmann constant	ψ	stream function
Kn	Knudsen number ($Kn = l/d_p$)	ρ	density of fluid
l	mean free path of the surrounding gas	θ	non-dimensional temperature ($\theta = (T - T_\infty)/(T_w - T_\infty)$)
N	concentration		
p	static pressure of the fluid		
Pr	Prandtl number ($Pr = \nu/\alpha$)	<i>Subscripts</i>	
p_∞	static pressure in the undisturbed fluid	f	fluid
Sc	Schmidt number ($Sc = \nu/D_B$)	p	particle
T	static temperature of the fluid	w	condition at the wall
T_∞	static temperature in the undisturbed fluid	∞	condition in the undisturbed fluid
$\Delta\hat{T}$	non-dimensional temperature difference ($\Delta\hat{T} = (T_w - T_\infty)/T_\infty$)		
u	velocity component in the x -direction	<i>Superscripts</i>	
v	velocity component in the y -direction	'	differentiation with respect to η
V_d	deposition velocity	^	non-dimensional deposition velocity
x	coordinate measured along the plate		
y	coordinate measured normal to the plate		

produces this movement of particles is called thermophoretic force and the resulting motion of particles is called thermophoresis (details about theories and experiments on thermophoresis are given in Section 2). If the fluid motion is turbulent, additional mechanisms of particle transport are provided by diffusion due to turbulent eddies and turbophoresis. Deposition of particles is also modified by the presence of roughness elements on the surface on which deposition takes place. All such mechanisms are included in the unified advection-diffusion theory (Guha (1997, 2008a, 2008b)) of particle transport and deposition applicable for laminar as well as turbulent flow. The paper by Guha (1997) also contains the first solution of thermophoretic movement of particles suspended in a flowing fluid (forced convection) with the application of the unified advection-diffusion theory, unearthing complex interaction between thermophoresis and turbophoresis for certain sizes of particle.

In this paper, the motion of nano- to micro-sized aerosol particles (particle diameter in the range 1 nm–5 μm) as a result of (laminar) natural convection of the base fluid is considered. Since natural convection arises due to a temperature difference between the bounding surface and the quiescent fluid, Brownian diffusion and thermophoresis are inextricably linked. Nevertheless, an artefact has been devised in this paper to separate the effects of Brownian diffusion and thermophoresis. Four flow configurations (Fig. 1) are considered for the sake of developing a comprehensive physical picture: natural convective boundary layer developing in the upward direction (i.e. against the direction of gravity) along a heated vertical plate, that developing in the downward direction along a cooled vertical plate, that developing above a heated horizontal plate, and a natural convective boundary layer developing beneath a cooled horizontal plate. Only a few such studies have been published previously [Epstein et al. (1985), Nazaroff and Cass (1987), and Tsai (2001) for deposition on a vertical plate, and Guha and Samanta (2014) for deposition on a horizontal plate], but all of them employed older expressions [e.g. the well-known formula given by Talbot et al. (1980)] for computing the thermophoretic force. Recently, however, Sagot et al. (2009) and Brugi re et al. (2013) have concluded that the expression for thermophoretic force coefficient proposed by Beresnev and Chernyak (1995) provides the best agreement with experimental measurements. This paper, therefore, investigates in detail how the various expressions of thermophoretic force coefficient affect the predicted natural convective motion of nano- to micro-sized aerosol particles. There appears to be no available experimental data for thermophoresis in natural convective flow on a vertical plate or a horizontal plate. The number of available theoretical studies on this topic is also very limited (as explained above). It is in this context that we have attempted to provide a comprehensive theoretical treatment of the subject-matter.

The mathematical treatment for the determination of fluid flow field due to natural convection along a vertical plate is standard and is available in any textbook on convection (e.g. Burmeister, 1983). In contrast, the literature on the analysis of

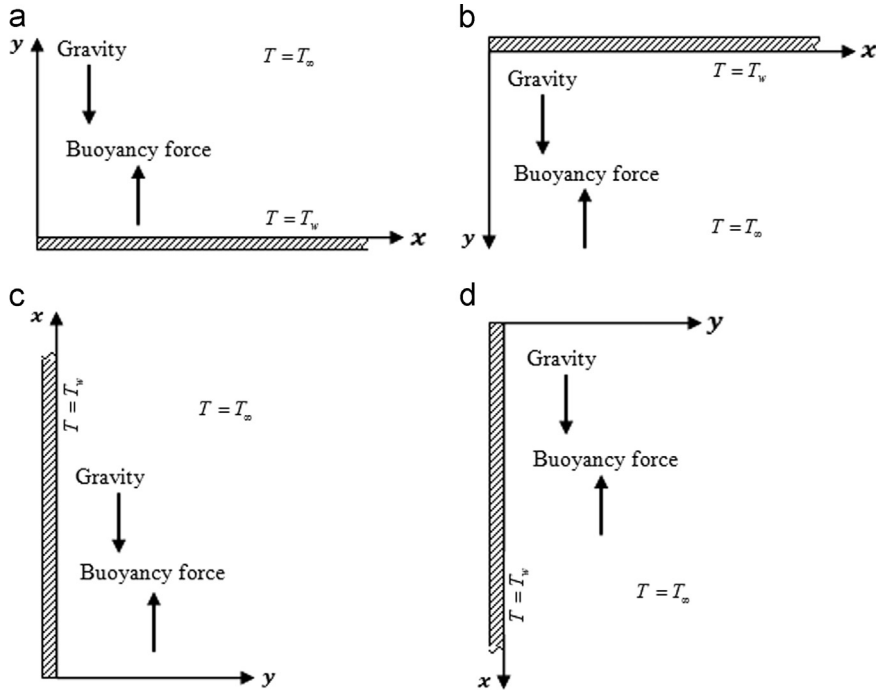


Fig. 1. Physical model and coordinate system. (a) Heated horizontal plate facing upward ($T_w > T_\infty$). (b) Cold horizontal plate facing downward ($T_\infty > T_w$). (c) Heated vertical plate ($T_w > T_\infty$). (d) Cold vertical plate ($T_\infty > T_w$).

laminar natural convection over a horizontal plate is rather limited (Stewartson, 1958; Rotem and Claassen, 1969; Schlichting and Gersten, 2004; Samanta and Guha, 2012). The natural convection boundary layer above a horizontal plate is formed indirectly because of an induced pressure gradient and thus it is termed as ‘indirect natural convection’ (Schlichting and Gersten, 2004). In the standard analysis of natural convection on a vertical plate, it is assumed that $\partial p/\partial x = -\rho_\infty g$ and $\partial p/\partial y = 0$. On the other hand, the boundary layer on a horizontal plate due to natural convection is such that $\partial p/\partial y \neq 0$ and $\partial p/\partial x$ cannot be neglected inside the boundary layer (even when $\partial p_\infty/\partial x$ is zero). Particle transport and deposition on both vertical and horizontal plates are analyzed in the present paper.

2. Mathematical formulation for horizontal plate

Consider steady, laminar natural convection boundary layer flow of a viscous and incompressible fluid past a semi-infinite horizontal plate. The plate is subjected to a constant wall temperature T_w . The quiescent ambient fluid is maintained at a uniform temperature T_∞ and pressure p_∞ . The flow configuration is presented in Fig. 1(a).

The boundary layer equations in dimensional form governing natural convection flow over a horizontal plate under Boussinesq approximation are

Continuity equation:

$$\frac{\partial u}{\partial x} + \frac{\partial v}{\partial y} = 0 \tag{1}$$

x-momentum equation:

$$u \frac{\partial u}{\partial x} + v \frac{\partial u}{\partial y} = -\frac{1}{\rho} \frac{\partial p}{\partial x} + \nu \frac{\partial^2 u}{\partial y^2} \tag{2}$$

y-momentum equation:

$$-\frac{1}{\rho} \frac{\partial p}{\partial y} + g\beta(T - T_\infty) = 0 \tag{3}$$

Energy equation:

$$u \frac{\partial T}{\partial x} + v \frac{\partial T}{\partial y} = \alpha \frac{\partial^2 T}{\partial y^2} \tag{4}$$

The motion of small particles in such a flow field is governed by the following equation:

$$u \frac{\partial N}{\partial x} + v \frac{\partial N}{\partial y} = D_B \frac{\partial^2 N}{\partial y^2} + D_T \frac{\partial}{\partial y} \left(\frac{1}{T} \frac{\partial T}{\partial y} N \right) \quad (5)$$

Guha (1997, 2008a, 2008b) has derived, from fundamental conservation equations of mass and momentum for the particles, a unified Eulerian advection-diffusion theory in which the various mechanisms of particle transport and deposition arise automatically. The equations are valid for laminar to turbulent flow and for a wide range of particle size (nanoparticles to large millimeter-sized particles). The theory incorporates the effects of inertia, Brownian diffusion, thermophoresis, turbophoresis, electrical and other body forces, gravity, shear-induced lift, surface roughness, and corrections due to Knudsen effect or finite slip Reynolds number. These equations reduce to the well-known relations in the appropriate limits. Thus, for example, Fick's law of diffusion or the currently popular equations for the motion of nanoparticles can be viewed as subsets of the unified advection-diffusion theory derived. Experiments show that the deposition velocity varies differently with the size of particle in different ranges of particle size and it can vary by several orders of magnitude as particle size is altered. In the past, separate theories were needed in different particle size ranges and it would have been difficult to apply the theories to flow situations that are different from the situations for which the parameters of the theories were tuned. The unified advection-diffusion theory thus settles the quest over previous 70 years in the field for a physics-based explanation for the observed complex behavior of particle transport.

In the literature, often deposition “velocities” are determined separately for various physical mechanisms and then added to calculate the overall deposition rate. The work of Guha (1997) takes a more fundamental approach in which the forces acting on particles are properly accounted for and are vectorially added in the momentum equation. The overall deposition rate is then computed from the solution of fundamental conservation equations. This ought to be a superior approach than the more usual linear superposition of the respective “velocities”.

The present version of particle concentration equation (5) is a special case of the generalized particle transport equation of Guha (1997). The relevant mechanisms of particle transport and deposition for the present work include Brownian diffusion and thermophoresis. Since laminar natural convection is considered here, the terms arising out of the interaction of the particle and fluid turbulence are not retained. In this work fluid velocities are used in the LHS of Eq. (5) instead of separate particle velocities; hence the equation would be valid only for small particles; however, the original equation used by Guha (1997) for the inertial relaxation time includes necessary correction to Stoke's drag law due to large slip velocity between the two phases. Effect of any body forces (including gravity) on the particles is not considered in the present study.

Here x and y are dimensional coordinates along and normal to the plate, u and v are the velocity components in the x and y directions, p is the static pressure, g is the gravitational acceleration (only magnitude is to be considered, the sign is incorporated in the analysis), β is the coefficient of thermal expansion at the reference temperature, ρ , ν and α are the density, kinematic viscosity and thermal diffusivity of the fluid, respectively, and D_B is the Brownian diffusivity. D_T represents the coefficient of diffusion due to temperature gradient and is given by

$$D_T = D_B(1 + \kappa/kT) \quad (6)$$

The Brownian diffusivity D_B in Eqs. (5) and (6) is given by the Einstein equation incorporating the Cunningham correction for rarefied gas effects:

$$D_B = \left(\frac{kT}{3\pi\mu d_p} \right) C_c \quad (7)$$

where k is the Boltzmann constant, T is the absolute temperature, μ is the dynamic viscosity of the fluid, $C_c = 1 + Kn[2.514 + 0.8\exp(-0.55/Kn)]$ is the Cunningham correction factor and Kn is the Knudsen number defined by $Kn \equiv l/d_p$, where l is the mean free path of the surrounding gas and d_p is the diameter of a particle. l is calculated by the expression $l = \sqrt{\pi/2}\mu(1/\sqrt{\rho p})$.

Equation (6), which was mathematically derived by Guha (1997), shows that the thermal drift has a “stressphoretic” component and a thermophoretic component (the term containing κ). The “stressphoretic” component of the thermal drift of the particles arises from the evaluation of the term ∇p_p in particle momentum equation (Guha, 1997), where p_p is the partial pressure of the particle cloud. Theoretical determination of the thermophoretic force coefficient κ usually involves a single particle. κ depends on the particle size and on the ratio ($\lambda_r \equiv \lambda_f/\lambda_p$) of the thermal conductivity of the fluid (λ_f) and that of the particle (λ_p). Since the publication of the pioneering work on thermophoresis by Tyndall (1870), who described the migration of dust particles away from a heated surface forming a dust-free layer close to the surface, many theories have been constructed to describe the phenomenon (Epstein, 1929; Waldmann, 1959; Brock, 1962; Dwyer, 1967; Ivchenko and Yalamov, 1970; Sone, 1972; Talbot et al., 1980; Sone and Aoki, 1981; Yamamoto and Ishihara, 1988; Beresnev and Chernyak, 1995). The theoretical treatments are based on continuum equations with slip-corrected boundary conditions, phenomenological equations based on postulates of irreversible thermodynamics or various forms of the kinetic theory. Epstein (1929) was the first to use the analysis by Maxwell (1879) for gaseous thermal creep in order to develop a theory for the thermophoretic force on a spherical particle in a gas with a temperature gradient. Later theories have incorporated features required to deal with the effect of particle thermal conductivity and large particle Knudsen number (giving rise to slip, transitional and free molecular regimes). In the continuum limit ($Kn \rightarrow 0$), Epstein's formula shows that κ depends on λ_r (κ decreases as λ_r decreases) but is independent of Kn . In the free molecule limit ($Kn \rightarrow \infty$), Waldmann's expression

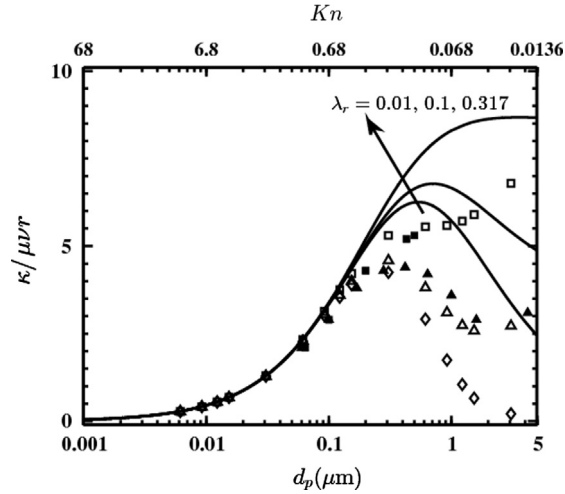


Fig. 2. Thermophoretic force coefficient (κ) for various values of particle diameter (d_p) at selected values of λ_r . The solid lines are the interpolation of Talbot et al. (1980). The open symbols are the data from Beresnev and Chernyak (1995). (Keys: \square $\lambda_r = 0.317$ (Beresnev and Chernyak, 1995), \triangle $\lambda_r = 0.1$ (Beresnev and Chernyak, 1995), \diamond $\lambda_r = 0.01$ (Beresnev and Chernyak, 1995), \blacktriangle $\lambda_r = 0.1$ (Sagot et al., 2009), \blacksquare $\lambda_r = 0.317$ (Brugi re et al., 2013). (For all calculations $l = 68$ nm).

demonstrates that κ is independent of λ_r (κ varies as $1/Kn$ in this limit). In the slip flow and transition regimes (where Kn takes intermediate values), κ is a function of both λ_r and Kn . Developing a reliable theory for these regimes is a challenging task. More details are available in the review articles by Talbot et al. (1980), Bakanov (1991), and Zheng (2002).

For the purpose of the present work two theoretical expressions for κ have been considered: the expression given by Talbot et al. (1980) and that given by Beresnev and Chernyak (1995). An important aspect of both expressions is that they are intended for the entire range of the Knudsen number (i.e. from the continuum to the free molecule regime). The expression proposed by Talbot et al. (1980) is the most used so far; the expression proposed by Beresnev and Chernyak (1995) is shown by Sagot et al. (2009) to be more accurate in the transition regime ($0.05 < Kn < 5$).

Talbot et al. (1980), by slightly adjusting the values of thermal slip coefficient (C_s) and momentum exchange coefficient (C_m) in Brock's theory (Brock (1962)), which was originally developed to model the continuum and slip flow regime ($Kn < \sim 0.05$) and based on the continuum equations with slip-corrected boundary conditions, proposed an interpolation formula intended for all Knudsen numbers including the free molecular regime. The thermophoretic force coefficient (κ) given by Talbot et al. (1980) is

$$\kappa = \frac{2.34(6\pi\mu\nu r)(\lambda_r + 4.36Kn)}{(1 + 6.84Kn)(1 + 8.72Kn + 2\lambda_r)}. \quad (8)$$

This expression for κ proposed by Talbot et al. has been widely used in the literature for all regimes of Knudsen number ($0 < Kn < \infty$). Recent experimental measurements (Sagot et al., 2009; Brugi re et al., 2013; Sagot, 2013), however, suggest that the thermophoretic force predicted by using the expression of Talbot et al. gives considerably higher values, especially in the transition regime ($0.05 < Kn < 5$).

Beresnev and Chernyak (1995) developed an approach to predict the values of thermophoretic force coefficient (κ) of a spherical particle at arbitrary Knudsen number. Their theory is based on the linearized Bhatnagar–Gross–Krook (BGK) (Bhatnagar et al., 1954) and S model kinetic equations (Shakhov, 1968). The analysis of Beresnev and Chernyak (denoted as B&C in a few places of this paper) introduced accommodation factors for energy (α_E) and momentum (α_r) to consider the manner in which colliding molecules are reflected by the particle. The thermophoretic force coefficient (κ) as given by Beresnev and Chernyak (1995) considering complete accommodation ($\alpha_E = \alpha_r = 1$) is

$$\kappa = \frac{\pi}{Kn} \mu \nu r \left[\frac{\lambda_r f_{11} + f_{21}}{\lambda_r f_{31} + (\lambda_r + 5Kn) f_{41}} \right] \quad (9)$$

where f_{ij} are coefficients tabulated for various Knudsen numbers (Kn) in the original paper by Beresnev and Chernyak (1995).

Eqs. (8) and (9) both tend to the free molecule limit of Waldmann (1959) as $Kn \rightarrow \infty$, and to the continuum limit of Epstein (1929) as $Kn \rightarrow 0$. The discrepancies in the values of κ as given by the two Eqs. (8) and (9) are, however, significant in the transition and slip flow regime, particularly at small values of λ_r . A comparison of the values of κ obtained from Eqs. (8) and (9) is presented in Fig. 2 which also includes recent experimental data. The experiments of Sagot et al. (2009) and Brugi re et al. (2013), within the range of parameters investigated, tend to support the expression for κ proposed by Beresnev and Chernyak (B&C). Sagot et al. suggest that better agreement with the B&C theory would be obtained if the value of energy accommodation coefficient α_E is adjusted to 0.93 instead of unity. The experimental data of Sagot et al. (2009) were, however, obtained only for one value of thermal conductivity ratio ($\lambda_r = 0.1$). The experimental data of Brugi re et al.

Table 1Values of the function $\kappa/\mu\nu r$ using Eq. (9) at $\lambda_r = 0.001$.

d_p (μm)	$Kn = l/d_p$	$\kappa/\mu\nu r$	d_p (μm)	$Kn = l/d_p$	$\kappa/\mu\nu r$	Comment
0.0061	11.1475	0.279	1.2277	0.0554	0.8619	} Reversed thermophoresis
0.0092	7.3913	0.4147	1.5346	0.0443	0.4433	
0.0123	5.5285	0.5483	3.0692	0.0222	-0.0792	
0.0153	4.4444	0.6777	6.1384	0.0111	-0.0754	
0.0307	2.215	1.2836	9.2076	0.0074	-0.0388	
0.0614	1.1075	2.2776	12.2768	0.0055	-0.0184	
0.0921	0.7383	3.0116	15.346	0.0044	-0.006	
0.1228	0.5537	3.5339	30.6919	0.0022	0.0188	
0.1535	0.443	3.8884	61.3838	0.0011	0.0307	
0.3069	0.2216	4.2132	92.0757	0.0007	0.0347	
0.6138	0.1108	2.819	122.7677	0.0006	0.0366	
0.9208	0.0738	1.5979	153.4596	0.0004	0.0378	

(2013) is also limited as they cover only a small part of the important transition regime. It is to be noted that both Sagot et al. and Brugi re et al. have given data for thermophoretic velocity. For plotting the experimental data in Fig. 2, the thermophoretic velocity data need to be converted to thermophoretic force. This conversion is achieved by assuming that the thermophoretic force is balanced by the drag force which is calculated using the expression given by Beresnev and Chernyak (1995) (their Eq. (30)).

A continuous function (Eq. (8)) for the thermophoretic force coefficient (κ) is provided by Talbot et al. It allowed us to calculate the value of κ for any value of the particle diameter. However, the expression for κ (Eq. (9)) provided by Beresnev and Chernyak contains coefficients that are to be obtained from the numerical solution of the BGK and S model equations. Beresnev and Chernyak have provided values of the coefficients for a few discrete values of particle diameter. We have calculated the values of κ at these points which fall within the range of particle diameter $0.001 \leq d_p \leq 5 \mu\text{m}$ ($68 \geq Kn \geq 0.0136$). This is why we have shown B&C results at discrete points but Talbot et al. results by continuous lines in Fig. 2 and in the subsequent figures. Incidentally, this aspect also makes the expression of Talbot et al. easier to apply for practical calculations.

An interesting feature of a few theories of thermophoresis is that when λ_r is small, the direction of the thermophoretic force may be reversed for some low values of Kn . When λ_r is small ($\lambda_r \ll 1$), the temperature on the particle surface is almost uniform and Maxwell's thermal creep flow is negligible. A higher order effect may then determine the flow field and the force on the particle. Reversed thermophoresis, in which the force acts along the temperature gradient (i.e. from low to high temperatures), was, for example, predicted by Dwyer (1967) and Sone (1972). We have computed the values of κ using the expression of Beresnev and Chernyak (1995) for a low value of thermal conductivity ratio ($\lambda_r = 0.001$) as an example; these values are given in Table 1. It can be seen from Table 1 that for $\lambda_r = 0.001$ and $0.0044 \leq Kn \leq 0.0222$, the theory of Beresnev and Chernyak predicts reversed thermophoresis. The extent of reversed thermophoresis that arises according to the Beresnev and Chernyak theory is, however, much less than what is obtained by the theories of Sone and Aoki (1981), and Yamamoto and Ishihara (1988), who solved the original BGK equation. Equation (8), the expression given by Talbot et al. (1980), on the other hand, does not admit reversed thermophoresis for any values of the parameters. Though theoretically interesting, reversed thermophoresis has not so far been demonstrated experimentally.

Having discussed various theories for thermophoresis, it would be relevant to briefly mention about the experiments available. The experimental study of thermophoretic movement of aerosol particles is usually based on one of the following three techniques: (a) measurement of thermophoretic force, (b) measurement of thermophoretic velocity, or (c) measurement of deposition efficiency. Measurement of thermophoretic force is based on either a force balance within a modified Millikan cell (Jacobsen and Brock, 1965) or using an electrodynamic balance (Li and Davis, 1995). Prodi et al. (1979) developed a set-up for the experimental determination of thermophoretic velocity, which was designed to measure the deviation of a particle's trajectory due to an imposed temperature gradient in a jet flow. Recently, Brugi re et al. (2013) have reported the development of a new device called the radial flow thermophoretic analyzer for measuring the thermophoretic velocity. Determination of deposition efficiency is based on the measurement of aerosol particle concentration upstream and downstream of the test section. Sagot et al. (2009) measured aerosol deposition efficiency for flow through a concentric tube annulus in the presence of an imposed temperature gradient. An analytical model was developed to calculate thermophoretic velocity from the measured deposition efficiency. Details on relative advantages and disadvantages of various measurement techniques have been documented by Zheng (2002) and Sagot et al. (2009). In this connection, it may be noted that caution is needed to compare and understand various published theoretical and experimental works on thermophoretic motion of particles since different researchers may have used different methods for inter-conversion between thermophoretic force and thermophoretic velocity.

Most of the reported experiments on particle deposition affected by thermophoresis are for cases where the fluid convective velocity is externally imposed (i.e. forced convection). There are a few available studies for natural convection inside a cavity. Unfortunately there appears to be no available experimental data for thermophoresis in natural convective flow on a vertical plate or a horizontal plate, which is the subject-matter of the present theoretical study.

The boundary conditions for the solution of Eqs. (1)–(5) are

$$\begin{aligned} \text{at } y=0, \quad u=0, \quad v=0, \quad T=T_w, \quad N=0; \\ \text{at } y \rightarrow \infty, \quad u \rightarrow 0, \quad p \rightarrow p_\infty, \quad T \rightarrow T_\infty, \quad N \rightarrow N_\infty. \end{aligned} \tag{10}$$

We introduce a stream function ψ defined by

$$u = \frac{\partial \psi}{\partial y} \quad \text{and} \quad v = -\frac{\partial \psi}{\partial x} \tag{11}$$

which automatically satisfies the continuity equation (1).

We are then left with the following four equations:

$$\frac{\partial \psi}{\partial y} \frac{\partial^2 \psi}{\partial x \partial y} - \frac{\partial \psi}{\partial x} \frac{\partial^2 \psi}{\partial y^2} = -\frac{1}{\rho} \frac{\partial p}{\partial x} + \nu \frac{\partial^3 \psi}{\partial y^3} \tag{12}$$

$$-\frac{1}{\rho} \frac{\partial p}{\partial y} + g\beta(T - T_\infty) = 0 \tag{13}$$

$$\frac{\partial \psi}{\partial y} \frac{\partial T}{\partial x} - \frac{\partial \psi}{\partial x} \frac{\partial T}{\partial y} = \alpha \frac{\partial^2 T}{\partial y^2} \tag{14}$$

$$\frac{\partial \psi}{\partial y} \frac{\partial N}{\partial x} - \frac{\partial \psi}{\partial x} \frac{\partial N}{\partial y} = D_B \frac{\partial^2 N}{\partial y^2} + D_T \frac{\partial}{\partial y} \left(\frac{1}{T} \frac{\partial T}{\partial y} N \right) \tag{15}$$

Using the generalized stretching transformation, the similarity forms of Eqs. (12)–(15) can be obtained as

$$\psi = \nu (Gr_x)^{1/5} f(\eta), \quad (p - p_\infty) = \rho \frac{\nu^2}{x^2} (Gr_x)^{4/5} h(\eta), \quad \theta(\eta) = \frac{(T - T_\infty)}{(T_w - T_\infty)}, \quad \phi(\eta) = \frac{N}{N_\infty} \tag{16}$$

where the similarity variable η is defined as $\eta = (y/x)(Gr_x)^{1/5}$ and $Gr_x = (g\beta(T_w - T_\infty)x^3)/\nu^2$ is the local Grashof number. The criterion for transition from laminar to turbulent flow in natural convection is expressed in terms of the Grashof number. For isothermal horizontal plates, the transition takes place at $Gr_x \sim 10^6$ (Faghri et al., 2010).

Substituting Eq. (16) into Eqs. (12)–(15), we obtain the following nonlinear ordinary differential equations:

$$f''' + \frac{3}{5}ff'' - \frac{1}{5}f'^2 + \frac{2}{5}\eta h' - \frac{2}{5}h = 0 \tag{17}$$

$$h' = \theta \tag{18}$$

$$\frac{1}{Pr}\theta'' + \frac{3}{5}f\theta' = 0 \tag{19}$$

$$\frac{1}{Sc}\phi'' + \frac{3}{5}f\phi' + \left(\frac{D_T}{\nu}\right) \left(\frac{\Delta \hat{T}}{1 + \Delta \hat{T}\theta}\right) \left(\theta''\phi + \theta'\phi' - \frac{\Delta \hat{T}}{1 + \Delta \hat{T}\theta}\theta'^2\phi\right) = 0 \tag{20}$$

Here $Pr = \nu/\alpha$ is the Prandtl number, $Sc = \nu/D_B$ is the Schmidt number, and $\Delta \hat{T} = (T_w - T_\infty)/T_\infty$ is the non-dimensional temperature difference. For $T_\infty = 300$ K and $(T_w - T_\infty) = 30$ K, $\Delta \hat{T}$ equals 0.1. A positive value of $\Delta \hat{T}$ implies that the heated plate faces upward; a negative $\Delta \hat{T}$ indicates that the cold plate faces downward.

Eqs. (17)–(20) are solved subject to the following boundary conditions:

$$\begin{aligned} \text{at } \eta=0, \quad f=0, \quad f'=0, \quad \theta=1, \quad \phi=0; \\ \text{at } \eta \rightarrow \infty, \quad f' \rightarrow 0, \quad h \rightarrow 0, \quad \theta \rightarrow 0, \quad \phi \rightarrow 1. \end{aligned} \tag{21}$$

The condition $\phi = 0$ at $\eta = 0$ is used as the boundary condition to reflect the perfectly absorbing characteristics of the surface. This is a reasonable assumption for small particles. For a proper formulation of the boundary condition for the particle concentration at the wall, one would have to resort to kinetic theory. More comments on the concentration boundary condition at the surface may be found in Guha (1997, p. 1530) and in Guha (2008a, Section 4). Related aspects of two-phase flow are given by Guha (1998a, 1998b, 1998c, 1994, 1992).

3. Mathematical formulation for vertical plate

Natural convection of the base fluid past a vertical plate is a well-studied phenomenon and the analysis can be found in many textbooks (Burmeister, 1983; Schlichting and Gersten, 2004). In this paper we investigate the motion of small particles, particularly the thermophoretic component, in the natural convective flow-field of the base fluid. The flow configuration is presented in Fig. 1(c). The governing equations for mass, momentum and energy in laminar natural convective flow over an isothermal vertical plate are given by

Continuity equation:

$$\frac{\partial u}{\partial x} + \frac{\partial v}{\partial y} = 0 \quad (22)$$

x-momentum equation:

$$u \frac{\partial u}{\partial x} + v \frac{\partial u}{\partial y} = g\beta(T - T_\infty) + \nu \frac{\partial^2 u}{\partial y^2} \quad (23)$$

y-momentum equation:

$$\frac{\partial p}{\partial y} = 0 \quad (24)$$

Energy equation:

$$u \frac{\partial T}{\partial x} + v \frac{\partial T}{\partial y} = \alpha \frac{\partial^2 T}{\partial y^2} \quad (25)$$

The motion of small particles in such a flow field is governed by the following equation:

$$u \frac{\partial N}{\partial x} + v \frac{\partial N}{\partial y} = D_B \frac{\partial^2 N}{\partial y^2} + D_T \frac{\partial}{\partial y} \left(\frac{1}{T} \frac{\partial T}{\partial y} N \right) \quad (26)$$

The boundary conditions for the solution of Eqs. (22)–(26) are

$$\begin{aligned} \text{at } y=0, \quad u=0, \quad v=0, \quad T=T_w, \quad N=0; \\ \text{at } y \rightarrow \infty, \quad u \rightarrow 0, \quad T \rightarrow T_\infty, \quad N \rightarrow N_\infty. \end{aligned} \quad (27)$$

The similarity forms of Eqs. (22)–(26) are given by

$$\psi = \nu(Gr_x)^{1/4} f(\eta), \quad \theta(\eta) = \frac{(T - T_\infty)}{(T_w - T_\infty)}, \quad \phi(\eta) = \frac{N}{N_\infty} \quad (28)$$

where the similarity variable η is defined as $\eta = (y/x)(Gr_x)^{1/4}$ and $Gr_x = (g\beta(T_w - T_\infty)x^3)/\nu^2$ is the local Grashof number. The fluid flow is laminar in the case of natural convection from a vertical isothermal plate if $Gr_x \leq 10^9$ (Faghri et al., 2010).

Substitution of (28) into the boundary layer Eqs. (22)–(25) gives the following set of ordinary differential equations:

$$f'' + \frac{3}{4}ff'' - \frac{1}{2}f'^2 + \theta = 0 \quad (29)$$

$$\frac{1}{Pr}\theta'' + \frac{3}{4}f\theta' = 0 \quad (30)$$

$$\frac{1}{Sc}\phi'' + \frac{3}{4}f\phi' + \left(\frac{D_T}{\nu}\right) \left(\frac{\Delta\hat{T}}{1+\Delta\hat{T}\theta}\right) \left(\theta'\phi' + \theta''\phi - \frac{\Delta\hat{T}}{1+\Delta\hat{T}\theta}\theta'^2\phi\right) = 0 \quad (31)$$

The corresponding boundary conditions are

$$\begin{aligned} \text{at } \eta=0, \quad f=0, \quad f'=0, \quad \theta=1, \quad \phi=0; \\ \text{at } \eta \rightarrow \infty, \quad f' \rightarrow 0, \quad \theta \rightarrow 0, \quad \phi \rightarrow 1. \end{aligned} \quad (32)$$

4. Orientation of the surface

The analysis in Section 2 is performed for laminar natural convective boundary flow above an upward-facing heated horizontal plate. It can be established by coordinate transformation that the same governing equations for the base fluid flow (Eqs. (17)–(19)) and their solutions would be valid for the case of laminar natural convection beneath a downward facing cold horizontal plate. The y-axis is chosen as positive in a direction normal to the plate for this case (Fig. 1(b)) and the local Grashof number is defined as $Gr_x = (g\beta(T_\infty - T_w)x^3)/\nu^2$. Similarly, the analysis in Section 3 is done for a heated vertical plate. Eqs. (29)–(30) for the base fluid flow can also be used for a cooled vertical plate if the coordinate system shown in Fig. 1(d) is used for the analysis and the local Grashof number is defined as $Gr_x = (g\beta(T_\infty - T_w)x^3)/\nu^2$. Therefore, to keep the present analysis valid for both heated and cold plates, the Grashof number is generically defined as $Gr_x = (g\beta|T_w - T_\infty|x^3)/\nu^2$.

The non-dimensional temperature difference $\Delta\hat{T}$ is considered positive when the fluid is heated by the plate (Fig. 1(a) and (c)) whereas it is negative when the fluid is cooled by the plate (Fig. 1(b) and (d)). The appropriate sign of $\Delta\hat{T}$ is to be incorporated in the solution of the particle concentration Eqs. (20) or (31). It is to be noted that only the third term (i.e. not all terms) in the LHS of Eq. (20) or (31) changes sign when the sign of $\Delta\hat{T}$ changes; hence the particle concentration equation needs to be solved afresh.

5. Non-dimensional deposition velocity

The particle deposition flux to the wall surface can be determined using the definition

$$J_w = D_B \left(\frac{\partial N}{\partial y} \right)_{y=0} \quad (33)$$

For a horizontal plate:

$$J_w = D_B \left(\frac{N_\infty}{x} \right) (Gr_x)^{1/5} \phi'(0) \quad (34)$$

For a vertical plate:

$$J_w = D_B \left(\frac{N_\infty}{x} \right) (Gr_x)^{1/4} \phi'(0) \quad (35)$$

The deposition velocity is defined as the particle flux divided by the free stream concentration,

$$V_d = J_w / N_\infty \quad (36)$$

For a horizontal plate:

$$V_d = \frac{D_B}{x} (Gr_x)^{1/5} \phi'(0) \quad (37)$$

For a vertical plate:

$$V_d = \frac{D_B}{x} (Gr_x)^{1/4} \phi'(0) \quad (38)$$

The local non-dimensional deposition velocity is defined as $\hat{V}_d = V_d x / \nu$, so that

For a horizontal plate:

$$\hat{V}_d = \frac{1}{Sc} \phi'(0) (Gr_x)^{1/5} \quad (39)$$

For a vertical plate:

$$\hat{V}_d = \frac{1}{Sc} \phi'(0) (Gr_x)^{1/4} \quad (40)$$

where $\phi'(0)$ depends on Sc , $\Delta\hat{T}$ and D_T for a fixed Pr .

6. Method of solution

For determining the fluid flow field, the system of Eqs. (17) and (19) for natural convection above a horizontal plate, subject to the boundary conditions (21), or the system of Eqs. (29)–(30) for laminar natural convection from a vertical plate, subject to the boundary conditions (32), is solved numerically for $Pr = 0.72$ (considering the fluid to be air) using the shooting iteration technique (Bradie, 2007). The system of equations is first reduced to first order ordinary differential equations which are then solved by marching forward in η . The boundary conditions for the first order equations at $\eta = 0$ are first guessed and these guessed values are updated in each iteration using the Newton method for simultaneous equations until agreement is reached with the prescribed boundary conditions at $\eta \rightarrow \infty$. The far-field asymptotic value of η during the numerical computation is taken to be 15 in order to ensure that the velocity and temperature profiles approach the quiescent ambient fluid conditions asymptotically.

In the present computations, a solution is said to converge when the difference between the specified and computed boundary values at $\eta \rightarrow \infty$ is less than 10^{-6} . In order to make sure that the numerical solution of fluid flow and heat transfer equations are not significantly dependent on the computational step size, a systematic study has been carried out with uniform step sizes equal to 0.001, 0.01 and 0.05. A fourth order Runge–Kutta method with step size of 0.01 was chosen for the numerical integration of governing differential equations.

Having described the numerical scheme for determining the fluid flow field we now turn our attention to the solution method for the particle continuity equation – Eq. (20) for natural convection over or underneath a horizontal plate and Eq. (31) for natural convection on a vertical plate. Since we consider only dilute mixtures (i.e. the volume of the dispersed phase is low) and one-way coupling (i.e., the particle motion depends on the fluid flow field but not vice versa), a knowledge of the converged velocity and temperature fields is required before the solution of the particle continuity equations (20) or (31). A value of $\phi'(0)$ is first guessed and this guessed value is updated in each iteration using Brent's method (Bradie, 2007).

A reference temperature of $T_\infty = 300$ K is used in the present study. The mean free path of air l is taken equal to 68 nm in all calculations. The particle diameter d_p is varied from 0.001 to 5 μm . The Schmidt number Sc correspondingly varies from 3.13 to 3.42×10^6 . For Sc values greater than unity, the concentration boundary layer is thinner than the hydrodynamic and thermal boundary layers. When the value of Sc is sufficiently large, the resulting concentration boundary layer is much thinner than the hydrodynamic and thermal boundary layers. Since the largest order (second order) term in the particle

continuity equation [Eq. (20) for a horizontal plate and Eq. (31) for a vertical plate] is multiplied by $1/Sc$, which becomes a very small number when Sc becomes large, the case would be similar to a singular perturbation problem. The particle concentration then changes rapidly close to the wall. An accurate and efficient solution for Eqs. (20) and (31) requires non-uniform computational step size with an extremely small size for the first computational cell ($\Delta\eta_1$) at the solid boundary. The value of the non-dimensional deposition velocity depends appreciably on the size of the first computational cell ($\Delta\eta_1$) and on the geometric progression (GP) ratio between the sizes of any two neighboring computational cells.

A reduction in either $\Delta\eta_1$ or GP ratio improves the accuracy of the solution but requires more computational time for convergence. A systematic grid independence test for both parameters was therefore undertaken along two strands (a) the GP ratio was progressively reduced from 1.2 to 1.01 while $\Delta\eta_1$ was maintained at a mean level (which was decreased significantly as the value of Sc increased), and (b) $\Delta\eta_1$ was progressively reduced while the GP ratio was maintained at a mean level. All computations are performed on a 64 bit Windows 7 platform with an Intel Core i5 desktop processor (3.26 GHz). The CPU time for computation increases approximately by a factor of 4 as the GP ratio decreases from 1.2 to 1.01 for a particular plate orientation, particle size, $\Delta\hat{T}$, $\Delta\eta_1$ and $\eta_{\infty,p}$ (computational boundary for particle continuity equation). The grid independence study showed that adopting a GP ratio between 1.02 and 1.05 would be a judicious choice considering necessary accuracy and affordable CPU time. A reduction in $\Delta\eta_1$ also increases the CPU time significantly. From a large number of such grid independence tests we have been able to formulate an empirical rule for adopting the optimum value of $\Delta\eta_1$: $(\Delta\eta_1)_{optimum} \sim (D_B \text{ in } m^2/s)/(100 \text{ } m^2/s)$. This developed prescription seems to work for all the computations presented in this work (both vertical and horizontal plates).

A convergence criterion of 10^{-6} is used for solving the particle continuity equation. From the above discussions, it would be clear that, depending on the value of Sc , many more grid points (particularly close to the solid wall) may be necessary for solving the particle continuity equation than what are required for solving the fluid flow field. The values of fluid flow variables such as f , θ and θ' are therefore determined at the new grid points through interpolation. In order to save CPU time, the value of $\eta_{\infty,p}$ is varied from 2 to 15 for the solution of particle continuity equation depending on the particle Schmidt

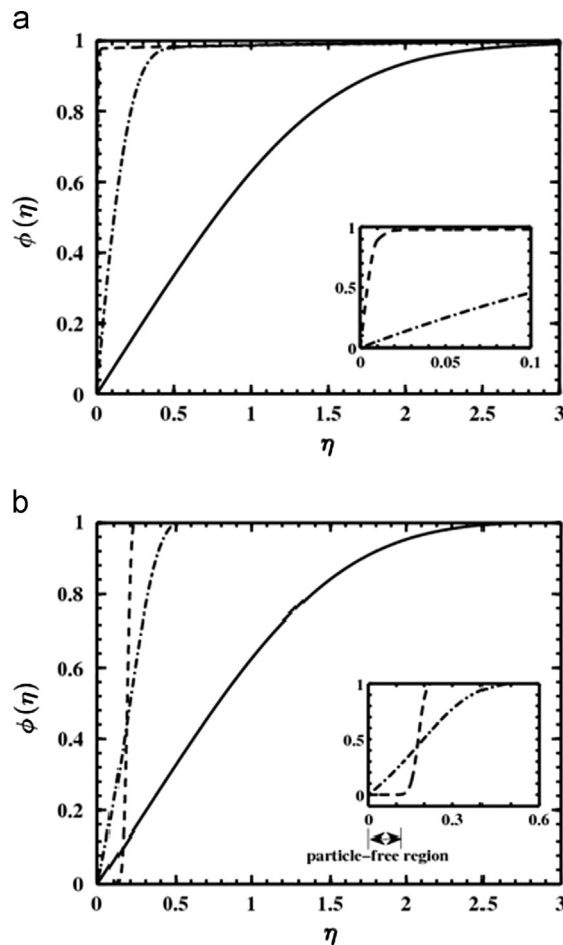


Fig. 3. Particle concentration profiles for an isothermal horizontal plate for various values of particle diameter d_p at $\lambda_r = 0.33$ (a) $\Delta\hat{T} = -0.05$, (b) $\Delta\hat{T} = 0.05$ (— $d_p = 0.001 \mu\text{m}$; -·-·- $d_p = 0.01 \mu\text{m}$; --- $d_p = 0.1 \mu\text{m}$. $\Delta\hat{T}$ is positive for natural convection above a heated horizontal plate, $\Delta\hat{T}$ is negative for natural convection beneath a cold horizontal plate. For all calculations $l = 68 \text{ nm}$. $\eta = y(Gr_x)^{1/5}/x$).

number (Sc). The computational challenge at high values of Sc may be appreciated by the fact that the CPU time increases dramatically at high values of Sc (while at $d_p = 1$ nm, the CPU time may be a few seconds, at $d_p = 5$ μm , the CPU time may rise to a few hours).

7. Results and discussion

The mechanisms of particle motion considered in the present study include Brownian diffusion, convection effects caused by fluid motion and thermophoresis caused by temperature gradient. Solutions are presented for particles of diameter 1 nm to 5 μm .

Figure 3 presents the non-dimensional self-similar particle concentration profiles $\phi(\eta)$ [$\phi(\eta) = N/N_\infty$] for an isothermal horizontal plate for various values of particle diameter d_p . It can be seen from the figure that the thickness of the concentration boundary layer decreases with an increase in particle diameter (d_p). This can be attributed to the fact that the Schmidt number (Sc), which indicates the ratio of the thicknesses of velocity and concentration boundary layers, increases with an increase in particle diameter ($Sc = \nu/D_B = (3\pi\mu\nu/kTC_c)d_p$). For a fluid with constant Pr and at a particular Grashof number Gr_x , the thickness of the velocity boundary layer is fixed and thus an increase in the value of Sc causes a decrease in the thickness of concentration boundary layer. A comparative analysis of Fig. 3(a) and 3(b) shows that, for a particular d_p , the thickness of the concentration boundary layer is slightly greater for a cooled horizontal plate as compared to a heated horizontal plate. From Fig. 3(b) it can be seen that for certain combinations of positive $\Delta\hat{T}$ and a large size of particles, thermophoresis drives the concentration boundary layer away to form a particle-free region close to a heated horizontal surface. This particle-free region is similar to the “dust-free layer” shown previously in the context of natural convection (Tyndall, 1870; Guha and Samanta, 2014) or in forced convection flow of aerosol over a plate (Talbot et al., 1980) and that over a wedge (García-Ybarra and Castillo, 1997).

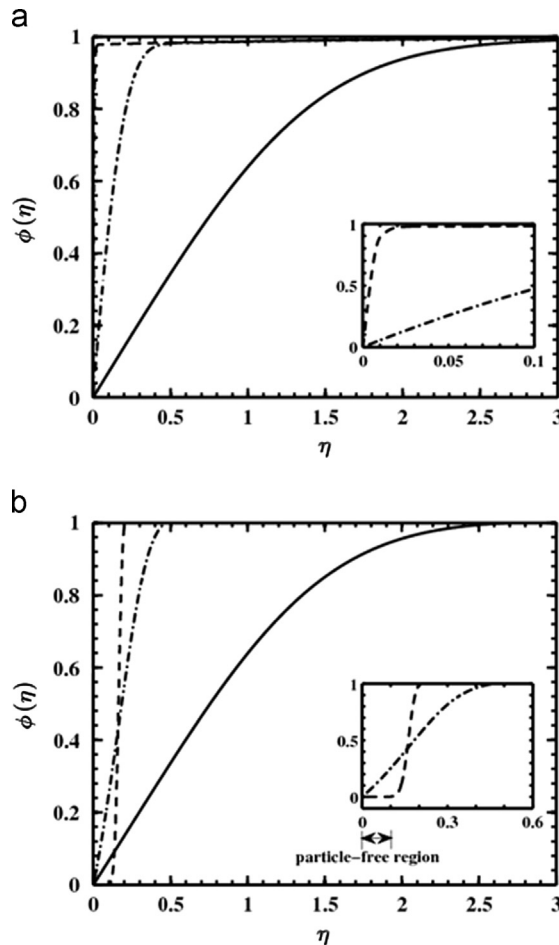


Fig. 4. Particle concentration profiles for an isothermal vertical plate for various values of particle diameter d_p at $\lambda_r = 0.33$ (a) $\Delta\hat{T} = -0.05$, (b) $\Delta\hat{T} = 0.05$ (— $d_p = 0.001 \mu\text{m}$; - · - · $d_p = 0.01 \mu\text{m}$; --- $d_p = 0.1 \mu\text{m}$). $\Delta\hat{T}$ is positive for natural convection on a heated vertical plate, $\Delta\hat{T}$ is negative for natural convection on a cold vertical plate. For all calculations $l = 68$ nm. $\eta = y(Gr_x)^{1/4}/x$.

Figure 4 presents the non-dimensional particle concentration profiles $\phi(\eta)$ in the natural convection boundary layer adjacent to a vertical plate for various values of particle diameter d_p . The qualitative trends of Fig. 4(a) and 4(b) are similar to the ones presented in Fig. 3(a) and 3(b). Figure 4(b) demonstrates that for certain combinations of positive $\Delta\hat{T}$ and large size of particles, a particle-free region may develop close to a heated vertical plate. A comparative analysis of Fig. 4(a) and 4(b) shows that, for a particular d_p , the thickness of the concentration boundary layer is slightly greater for a cooled vertical plate as compared to a heated vertical plate. Similarly, a comparative analysis of Figs. 3 and 4 will show that for a particular value of d_p and Gr_x , the thickness of concentration boundary layer for a horizontal plate is higher than that for a vertical plate.

Figure 5 presents the non-dimensional deposition velocity (\hat{V}_d) with particle diameter (d_p) as obtained from the numerical solution of particle concentration equation for a horizontal plate (Eq. (20)). Since Eq. (39) shows that $\hat{V}_d \propto (Gr_x)^{1/5}$, the composite variable $\hat{V}_d(Gr_x)^{-1/5}$ is plotted as the ordinate in Fig. 5: in this way data generated by comprehensive computations can be presented in a concise manner. In order to assess the consequence of using different expressions for the thermophoretic force coefficient (κ) on predicted deposition velocity, all computations are carried out using two different expressions for κ : (a) the expression proposed by Talbot et al. (Eq. (8)) and (b) that proposed by Beresnev and Chernyak (Eq. (9)).

Since the variable plotted along the y-axis (in Fig. 5 and in subsequent figures) is non-dimensional, it would be theoretically more appropriate to use a non-dimensional particle size along the x-axis, e.g. the Knudsen number. However, our engineering instinct suggests that a direct reference to the particle diameter may make the results more useful practically. In order to bridge the gap we have mentioned the gas mean free path in the figure captions so that the reader can easily convert the diameter to the corresponding Knudsen number.

Figure 6 presents the variation in non-dimensional deposition velocity (\hat{V}_d) with particle diameter (d_p) as obtained from the numerical solution of particle concentration equation for a vertical plate (Eq. (31)). The curves show a similar trend as in the case of particle deposition on an isothermal horizontal plate.

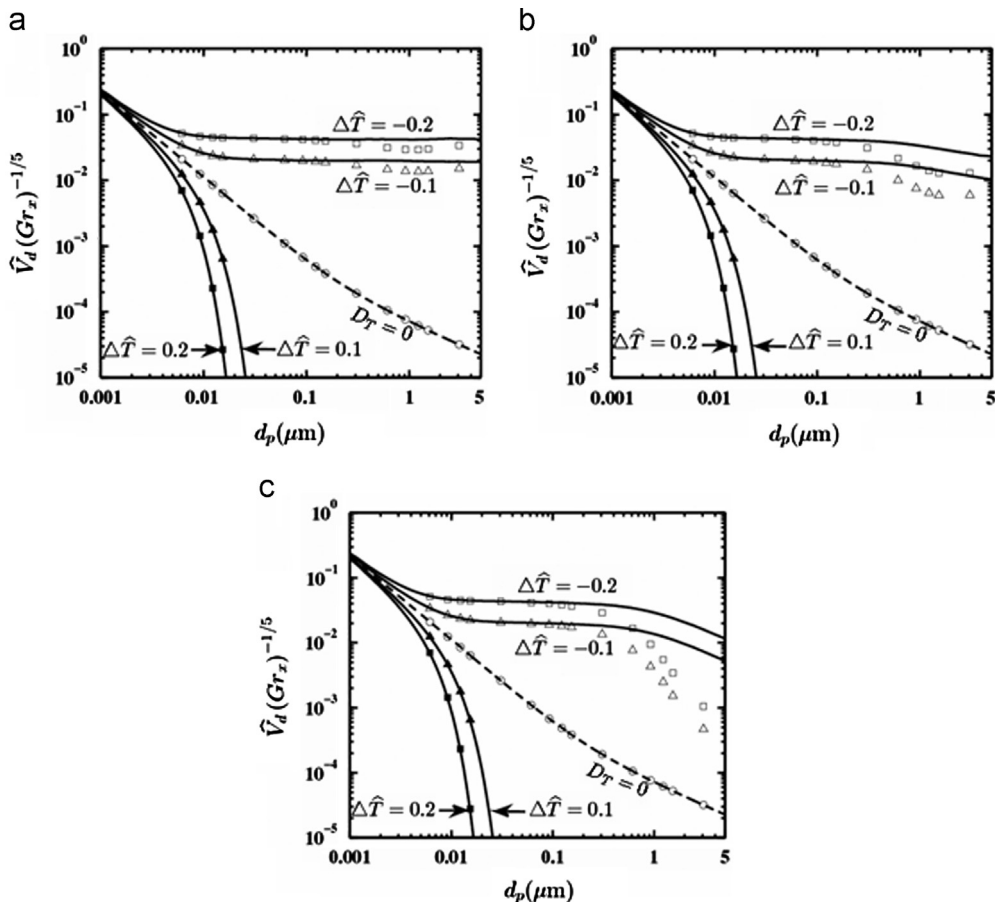


Fig. 5. Variation in non-dimensional deposition velocity (\hat{V}_d) with particle diameter d_p for an isothermal horizontal plate. $\Delta\hat{T}$ is positive for natural convection above a heated horizontal plate, $\Delta\hat{T}$ is negative for natural convection beneath a cold horizontal plate. For all calculations $l=68$ nm. The solid lines are the calculations incorporating the model of Talbot et al. The symbols are the calculations incorporating the model of Beresnev and Chernyak. Keys: $\square \Delta\hat{T} = -0.2$, $\triangle \Delta\hat{T} = -0.1$, $\circ D_T = 0$, $\blacktriangle \Delta\hat{T} = 0.1$, $\blacksquare \Delta\hat{T} = 0.2$. (a) $\lambda_r = 0.33$, (b) $\lambda_r = 0.1$ and (c) $\lambda_r = 0.01$.

The Brownian diffusivity of particles (D_B) decreases with an increase in particle diameter. The thermophoretic force coefficient κ mostly increases with particle diameter (with the B&C model, it may decrease slightly or even become negative over a small range of diameter in the transition regime particularly at small values of λ_r). The variation of $D_{B\kappa}$ or D_T is thus slightly more complex than that of D_B , though D_T generally decreases with increasing particle diameter when the diameter is small. Figures 5 and 6 show that the deposition velocity, in general, decreases with increasing diameter; however, for negative $\Delta\hat{T}$ and B&C model, the deposition velocity may increase slightly when the particle diameter is close to $5\ \mu\text{m}$.

When $\Delta\hat{T}$ is negative i.e. for a cold horizontal plate facing downward or for a cooled vertical plate, both Brownian diffusion and motion due to temperature gradient are towards the surface; hence these two effects aid each other to produce the overall deposition rate. When the particle size is very small (such as nanoparticles), the Brownian diffusion is the dominant mechanism. This is why the curves with various values of negative $\Delta\hat{T}$ approach one another for very small size of particles. As the particle size increases, D_B decreases and D_T also usually decreases but the decrease in D_B is faster. This is why thermophoresis component assumes dominance for large particles. In this regime, the deposition velocity is greater for higher values of $|\Delta\hat{T}|$. For a heated plate facing upward or heated vertical plate ($\Delta\hat{T}$ is positive), the particles tend to move towards the surface as a result of Brownian diffusion but tend to move away from the surface as a result of the temperature gradient. In this case, these two effects oppose each other to produce the overall deposition rate. Since D_T decreases at a lower rate than D_B with an increase in particle size, the effect of thermophoresis may dominate for large particles and the deposition velocity may decrease remarkably. This is why for both horizontal and vertical plates, the deposition velocity curves of Figs. 5 and 6 drop sharply towards the abscissa when $\Delta\hat{T}$ is positive.

A direct comparison of Figs. 5 and 6 show that the order of magnitude of non-dimensional deposition velocity for a horizontal plate is the same as that for a vertical plate for the same values of Prandtl number, particle size and temperature difference. Furthermore, the deposition velocity calculated by employing the expression of Talbot et al. (Eq. (8)) decreases continuously with increasing values of d_p . The rate of decrease in deposition velocity is small at large λ_r and negative $\Delta\hat{T}$. In the range $d_p \sim 1\text{--}5\ \mu\text{m}$, the deposition velocity decreases significantly with increasing radius, more so as λ_r is decreased. This decrease is more pronounced when the Beresenev and Chernyak model is used.

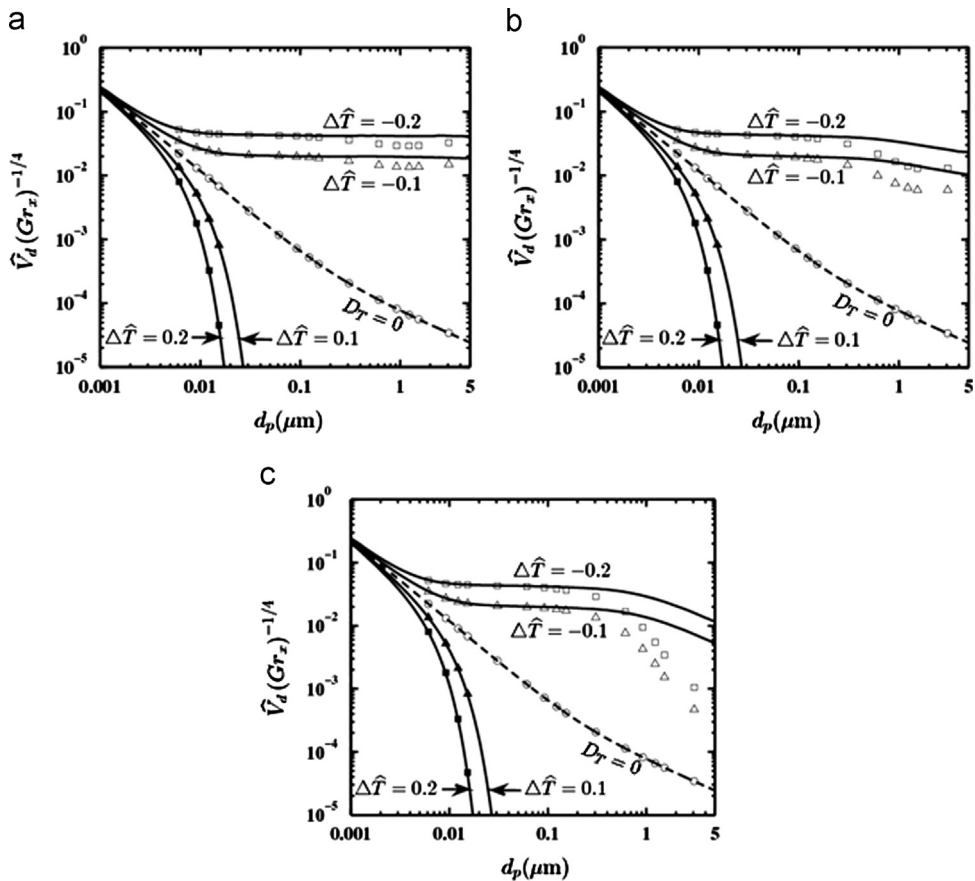


Fig. 6. Variation in non-dimensional deposition velocity (\hat{V}_d) with particle diameter d_p for an isothermal vertical plate. [$\Delta\hat{T}$ is positive for natural convection on a heated vertical plate, $\Delta\hat{T}$ is negative for natural convection on a cold vertical plate. For all calculations $l=68\ \text{nm}$. The solid lines are the calculations incorporating the model of Talbot et al. The symbols are the calculations incorporating the model of Beresenev and Chernyak. Keys: \square $\Delta\hat{T} = -0.2$, \triangle $\Delta\hat{T} = -0.1$, \circ $D_T = 0$, \blacktriangle $\Delta\hat{T} = 0.1$, \blacksquare $\Delta\hat{T} = 0.2$]. (a) $\lambda_r = 0.33$, (b) $\lambda_r = 0.1$ and (c) $\lambda_r = 0.01$.

For very small particles (e.g. $d_p \sim 1$ nm), deposition velocity is dominated by Brownian diffusion. That the contribution of thermal drift in determining the overall deposition rate is negligible for very small particles can be appreciated from Figs. 5 and 6 in which all curves, including the curve for $D_T = 0$ signifying the value of deposition velocity without thermal drift, approach the same value as $d_p \rightarrow 0$, or as $Kn \rightarrow \infty$ (please refer to the top-left corners of the graphs). In other words, in this limit of particle size, the deposition velocity is nearly insensitive to whatever expression for D_T is adopted.

We now want to examine in greater detail the contribution of thermophoresis in the overall deposition of aerosol particles in the natural convective flow of the base fluid. Therefore, two sets of differences are constructed: (i) the difference between the overall deposition velocity and that in the hypothetical case with $D_T = 0$; this difference signifying the role of thermophoresis in the context of other mechanisms of particle transport and deposition, and (ii) the difference between the overall deposition with κ given by Talbot et al. and that with κ given by Beresnev and Chernyak; this difference signifying the role of mathematical model in capturing the physical phenomenon called thermophoresis. Figures 7 and 8 correspond to the first set of difference quantities and Figure 9 corresponds to the second set. In order to save space we have presented results only for the horizontal plate (that too only for a fixed $\Delta\hat{T}$) since the results are similar at other values of $\Delta\hat{T}$ and for the case of the vertical plate.

Both absolute and relative values of the difference quantities are considered and their definitions are given directly in the ordinates of Figs. 7–9 in a self-explanatory manner. Thermophoresis may enhance deposition velocity by several order of magnitude (particularly for large λ_r and large d_p) as can be seen from Figs. 7(b) and 8(b). For both expressions of κ (Eqs. (8) and (9)), the effect of thermophoresis in increasing deposition velocity increases as λ_r ($\lambda_r = \lambda_f/\lambda_p$) increases, as can be seen from Figs. 7(a) and 8(a). The expression for κ suggested by Talbot et al. invariably predicts higher values of particle deposition velocity at a particular value of temperature difference $\Delta\hat{T}$ and particle diameter d_p . This can also be examined from Fig. 2 where it is seen that the values of κ are always higher for a particular d_p and λ_r when Eq. (8) is used instead of Eq. (9). Figure 9 shows that the difference between the model of Talbot et al. and that of Beresnev and Chernyak is most pronounced for low λ_r and large d_p .

The experimental data of Brugière et al. (Fig. 2) were obtained for particles in the size range of 64–500 nm (64, 100, 200, 430, 500) and for two values of thermal conductivity ratio ($\lambda_r = 0.317$ and $\lambda_r = 0.252$, where $\lambda_r \equiv \lambda_f/\lambda_p$). The experimental

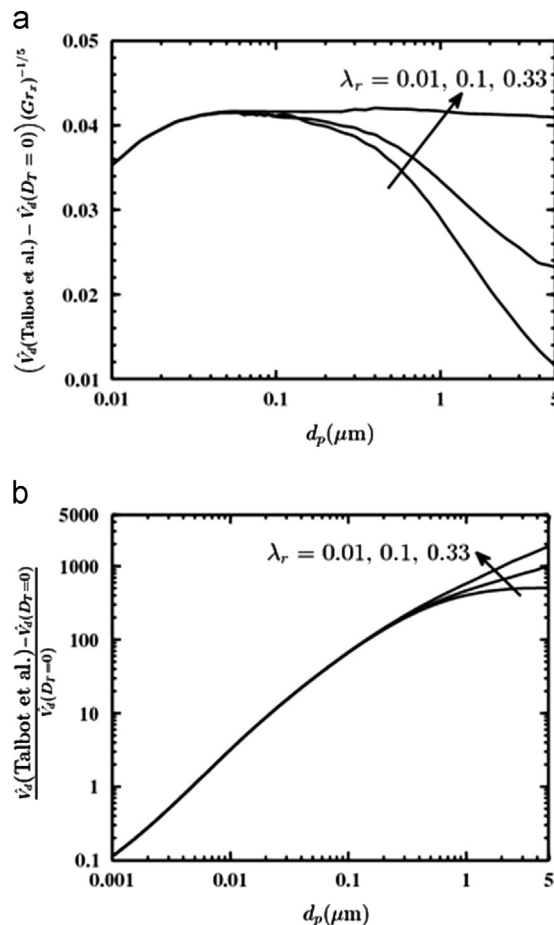


Fig. 7. Difference between overall deposition velocity and deposition velocity when $D_T = 0$ for $\Delta\hat{T} = -0.2$ and κ given by Eq. (8) in the case of a horizontal plate. (a) Absolute difference in deposition velocity and (b) relative difference in deposition velocity. For all calculations $l = 68$ nm.

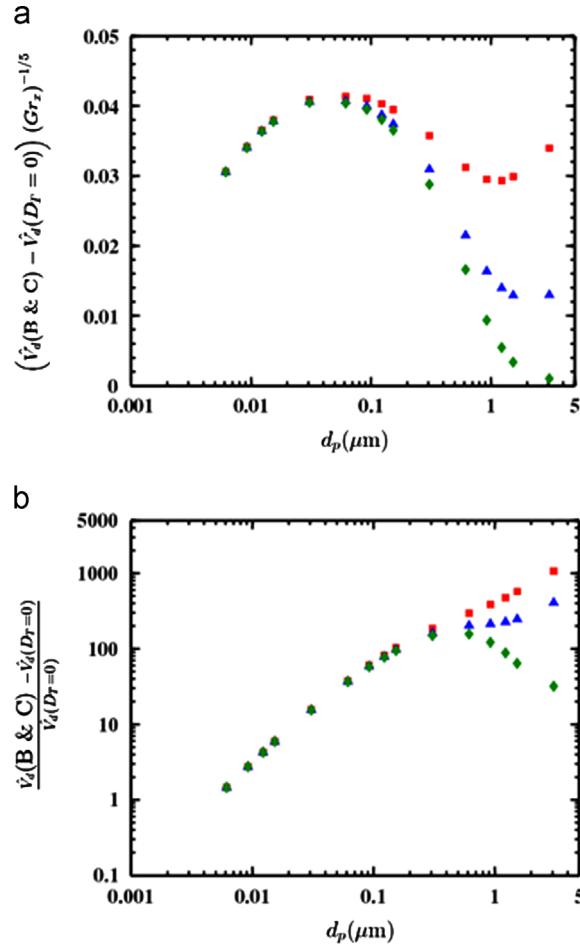


Fig. 8. Difference between overall deposition velocity and deposition velocity when $D_r = 0$ for $\Delta\hat{T} = -0.2$ and κ given by Eq. (9) in the case of a horizontal plate. (a) Absolute difference in deposition velocity and (b) relative difference in deposition velocity. (Keys: B & C Beresnev and Chernyak, $\lambda_r = 0.33$, $\blacktriangle \lambda_r = 0.1$, $\blacklozenge \lambda_r = 0.01$). (For all calculations $l=68$ nm).

data of Sagot et al. (Fig. 2) were obtained for particles in the size range 39–5130 nm for only one value of thermal conductivity ratio ($\lambda_r = 0.1$). These experiments indicate that the expression provided by Beresnev and Chernyak is superior to that given by Talbot et al. in the range of parameters investigated. Nevertheless, the work of Beresnev and Chernyak has caught the imagination of other researchers only in the last few years and there is no doubt that the work will be explored more thoroughly in the near future. The work of Talbot et al. has, on the other hand, become very popular and deeply entrenched both in the work of the research community as well as in computational software. One objective of the present paper is to assess the influence of the mathematical models of thermophoresis in the prediction of particle motion in natural convective flow. For this purpose, we have selected two models as the subject-matter: the model that has been used most so far and the model that is claimed to be most accurate so far. By looking into the comparative calculations, the researcher will be able to appreciate the influence of selecting a thermophoretic model in the prediction of particle motion in natural convective flow, and a code developer will be able to assess the necessity to revise one's computational codes.

8. Conclusions

The present work analyzes the effects of Brownian diffusion and thermophoresis on the motion of aerosol particles in steady laminar natural convection boundary layer flow on an isothermal plate. Four flow configurations are considered: (a) flow above a heated horizontal plate, (b) flow beneath a cold horizontal plate, (c) flow due to a heated vertical plate, and (d) that due to a cold vertical plate. Similarity solutions are formulated to determine the fluid flow field. The particle continuity equation is then solved to determine the non-dimensional deposition velocity on the surface.

It is found that the deposition velocity decreases with an increase in particle diameter d_p (i.e. an increase in particle Schmidt number Sc), and increases with a decrease in the value of non-dimensional temperature difference $\Delta\hat{T}$ (from positive to negative values).

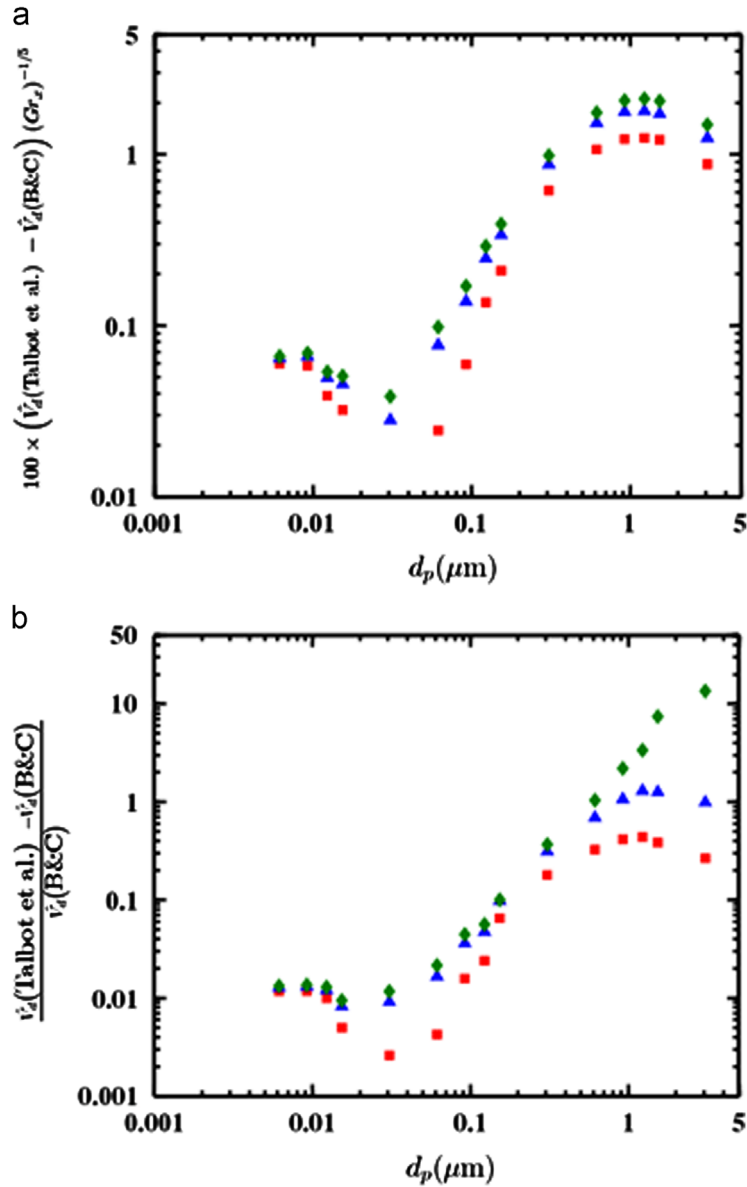


Fig. 9. Difference in non-dimensional deposition velocity using two different expressions for κ (Eqs. (8) and (9)) for an isothermal horizontal plate for $\Delta T = -0.2$. (a) Absolute difference in deposition velocity and (b) relative difference in deposition velocity. (Keys: B and C Beresnev and Chernyak, $\blacksquare \lambda_r = 0.33$, $\blacktriangle \lambda_r = 0.1$, $\blacklozenge \lambda_r = 0.01$). (For all calculations $l = 68$ nm).

The non-dimensional quantities $\hat{V}_d Sc / (Gr_x)^{1/4}$ and $\hat{V}_d Sc / (Gr_x)^{1/5}$ signify the gradient of particle concentration on the surface, $\phi'(0)$. The present study shows that, for the same values of Prandtl number, particle size and temperature difference, the value of the non-dimensional quantity $\hat{V}_d Sc / (Gr_x)^{1/4}$ (obtained from Eq. (40)) for vertical plates is comparable to the value of the non-dimensional quantity $\hat{V}_d Sc / (Gr_x)^{1/5}$ (obtained from Eq. (39)) for horizontal plates. This can be appreciated by comparing the corresponding magnitudes of deposition velocity given in Figs. 5 and 6.

It is shown that when the fluid is heated by the plate (heated vertical plate or heated horizontal plate facing upward), the thermal drift away from the surface decreases the overall deposition velocity which decreases drastically above a certain particle size. When the fluid is cooled by the plate (cold vertical plate or cold horizontal plate facing downward), thermal drift of particles assists Brownian diffusion. The curve with $D_T = 0$ is included in Figs. 5 and 6 to conceptually assess the importance of thermal drift on particle motion even though natural convective fluid flow field and thermal drift are inextricably linked through the same temperature difference between the plate and the quiescent fluid. Figures 7 (b) and 8 (b) show that thermophoresis may enhance deposition velocity by several orders of magnitude (particularly for large λ_r and large d_p).

The influence of various expressions for the thermophoretic force coefficient in determining the natural convective deposition rate is assessed in the present work. Two relations for the thermophoretic force coefficient are considered: (a) the commonly used expression proposed by Talbot et al. (1980) (Eq. (8)), and (b) the expression for thermophoretic force coefficient proposed by Beresnev and Chernyak (1995) (Eq. (9)). It is found that the non-dimensional deposition velocity obtained by using Eq. (8) is always higher than that obtained by using Eq. (9). Figure 9 shows that the difference between the model of Talbot et al. and that of Beresnev and Chernyak is most pronounced for low λ_r and large d_p . For example, at $d_p \sim 1 \mu\text{m}$, the Talbot et al. model may overpredict the deposition velocity by a factor 3, and at $d_p \sim 5 \mu\text{m}$, the Talbot et al. model may overpredict the deposition velocity by a factor 10. There is negligible difference between the two models when $d_p < 100 \text{ nm}$.

References

- Bakanov, S.P. (1991). Thermophoresis in gases at small Knudsen numbers. *Aerosol Science and Technology*, 15, 77–92.
- Beresnev, S., & Chernyak, V. (1995). Thermophoresis of a spherical particle in a rarefied gas: numerical analysis based on the model kinetic equations. *Physics of Fluids*, 7, 1743–1756.
- Bhatnagar, P.L., Gross, E.P., & Krook, M. (1954). A model for collision processes in gases. I. Small amplitude processes in charged and neutral one-component systems. *Physical Review*, 94, 511–525.
- Bradie, B. (2007). *A Friendly Introduction to Numerical Analysis*. Pearson Education: New Delhi.
- Brock, J.R. (1962). On the theory of thermal forces acting on aerosol particles. *Journal of Colloid Science*, 17, 768–780.
- Brugière, E., Gensdarmes, F., Ouf, F.-X., Yon, J., Coppalle, A., & Boulaud, D. (2013). Design and performance of a new device for the study of thermophoresis: the radial flow thermophoretic analyser. *Journal of Aerosol Science*, 61, 1–12.
- Burmeister, L.C. (1983). *Convective Heat Transfer*. John Wiley and Sons: New York.
- Dwyer, H.A. (1967). Thirteen-moment theory of the thermal force on a spherical particle. *Physics of Fluids*, 10, 976–984.
- Epstein, P.S. (1929). Zur Theorie des Radiometers. *Zeitschrift für Physik*, 54, 537–563.
- Epstein, M., Hauser, G.M., & Henry, R.E. (1985). Thermophoretic deposition of particles in natural convection flow from a vertical plate. *Journal of Heat Transfer*, 107, 272–276.
- Faghri, A., Zhang, Y., & Howell, J. (2010). *Advanced Heat and Mass Transfer*. Global Digital Press: Columbia.
- García-Ybarra, P.L., & Castillo, J.L. (1997). Mass transfer dominated by thermal diffusion in laminar boundary layers. *Journal of Fluid Mechanics*, 336, 379–409.
- Guha, A. (1997). A unified Eulerian theory of turbulent deposition to smooth and rough surfaces. *Journal of Aerosol Science*, 28, 1517–1537.
- Guha, A. (2008a). A generalized mass transfer law unifying various particle transport mechanisms in dilute dispersions. *Heat and Mass Transfer*, 44, 1289–1303.
- Guha, A. (2008b). Transport and deposition of particles in turbulent and laminar flow. *Annual Review of Fluid Mechanics*, 40, 311–341.
- Guha, A. (1998a). Computation, analysis and theory of two-phase flows. *The Aeronautical Journal*, 102(1012), 71–82.
- Guha, A. (1998b). A unified theory for the interpretation of total pressure and temperature in two-phase flows at subsonic and supersonic speeds. *Proceedings of the Royal Society*, 454, 671–695.
- Guha, A. (1998c). A simple, analytical theory for interpreting measured total pressure in multiphase flows. *ASME Journal of Fluids Engineering*, 120, 385–389.
- Guha, A. (1994). A unified theory of aerodynamic and condensation shock waves in vapour-droplet flows with or without a carrier gas. *Physics of Fluids*, 6(5), 1893–1913.
- Guha, A. (1992). Jump conditions across normal shock waves in pure vapour-droplet flows. *Journal of Fluid Mechanics*, 241, 349–369.
- Guha, A., & Samanta, S. (2014). Effect of thermophoresis on the motion of aerosol particles in natural convective flow on horizontal plates. *International Journal of Heat and Mass Transfer*, 68, 42–50.
- Ivchenko, I.N., & Yalamov, Y.I. (1970). Thermophoresis of aerosol particles in the nearly free molecular regime. *Fluid Dynamics*, 5, 355–358.
- Jacobsen, S., & Brock, J.R. (1965). The thermal force on spherical sodium chloride aerosols. *Journal of Colloid Science*, 20, 544–554.
- Li, W., & Davis, E.J. (1995). Measurement of the thermophoretic force by electrodynamic levitation: Microspheres in air. *Journal of Aerosol Science*, 26, 1063–1083.
- Maxwell, J.C. (1879). On stresses in rarified gases arising from inequalities of temperature. *Philosophical Transactions of the Royal Society of London*, 170, 231–256.
- Nazaroff, W.W., & Cass, G.R. (1987). Particle deposition from a natural convection flow onto a vertical isothermal flat plate. *Journal of Aerosol Science*, 18, 445–455.
- Prodi, F., Santachiara, G., & Prodi, V. (1979). Measurements of thermophoretic velocities of aerosol particles in the transition region. *Journal of Aerosol Science*, 10, 421–425.
- Rotem, Z., & Claassen, L. (1969). Natural convection above unconfined horizontal surfaces. *Journal of Fluid Mechanics*, 39, 173–192.
- Sagot, B., Antonini, G., & Buron, F. (2009). Annular flow configuration with high deposition efficiency for the experimental determination of thermophoretic diffusion coefficients. *Journal of Aerosol Science*, 40, 1030–1049.
- Sagot, B. (2013). Thermophoresis for spherical particles. *Journal of Aerosol Science*, 65, 10–20.
- Samanta, S., & Guha, A. (2012). A similarity theory for natural convection from a horizontal plate for prescribed heat flux or wall temperature. *International Journal of Heat and Mass Transfer*, 55(13–14), 3857–3868.
- Schlichting, H., & Gersten, K. (2004). *Boundary-Layer Theory*. Springer: New Delhi.
- Shakhov, E.M. (1968). Generalisation of the Krook kinetic relaxation equation. *Fluid Dynamics*, 3, 95–96.
- Sone, Y. (1972). Flow induced by thermal stress in rarefied gas. *Physics of Fluids*, 15, 1418–1423.
- Sone, Y., & Aoki, K. (1981). Negative thermophoresis: thermal stress slip flow around a spherical particle in a rarefied gas. In S.S. Fisher (Ed.), *Rarefied Gas Dynamics*. AIAA: New York, pp. 489–503.
- Stewartson, K. (1958). On the free convection from a horizontal plate. *Zeitschrift für angewandte Mathematik und Physik ZAMP*, 9, 276–282.
- Talbot, L., Cheng, R.K., Schefer, R.W., & Willis, D.R. (1980). Thermophoresis of particles in a heated boundary layer. *Journal of Fluid Mechanics*, 101, 737–758.
- Tsai, R. (2001). Aerosol particle transport in a natural convection flow onto a vertical flat plate. *International Journal of Heat and Mass Transfer*, 44, 867–870.
- Tyndall, J. (1870). On dust and disease. *Proceedings of the Royal Institution of Great Britain*, 6, 1–14.
- Waldmann, L. (1959). Über die Kraft eines inhomogenen Gases auf kleine suspendierte Kugeln. *Zeitschrift für Naturforschung*, 14a, 589–599.
- Yamamoto, K., & Ishihara, Y. (1988). Thermophoresis of a spherical particle in a rarefied gas of a transition regime. *Physics of Fluids*, 31, 3618–3624.
- Zheng, F. (2002). Thermophoresis of spherical and non-spherical particles: a review of theories and experiments. *Advances in Colloid and Interface Science*, 97, 255–278.